63-3-2

DASA 1344
USNRDL-TR-612
10 January 1963

EXPLODING WIRE PROGRAM
DETERMINATION OF THE TOTAL THERMAL RADIANT ENERGY EMITTED BY AN UNDERWATER EXPLODING WIRE

J. S. Hege

U.S. NAVAL RADIOLOGICAL DEFENSE LABORATORY
SAN FRANCISCO 24, CALIFORNIA

12ND, P7463

RADIOLOGICAL EFFECTS BRANCH
E. A. Schuert, Head

CHEMICAL TECHNOLOGY DIVISION
L. H. Gevantman, Head

ADMINISTRATIVE INFORMATION

The work reported was done as part of a project sponsored by Defense Atomic Support Agency, under NWER Program A7a, Subtask 10.001. The project is described (as Program A-1, Problem 2) in USNRDL Technical Program Summary for Fiscal Years 1963, 1964, and 1965, 1 November 1962.

Eugene P. Cooper
Eugene P. Cooper
Scientific Director

E. B. Roth, CAPT USN
Commanding Officer and Director

ABSTRACT

The total thermal radiation from an underwater spark has been determined by the measurement of the absolute radiation at two wavelengths as a function of time. Planck's law for thermal radiation was applied.

The spark was generated by electrically exploding a 5-mil. copper wire stretched between two submerged electrodes. The spark was assumed to be cylindrical with its length determined by the length of the wire.

The light measurements were made with two calibrated photoelectric tubes. Wavelengths of 407 and 610 millimicrons were selected with Farrand interference filters.

Values for the rates of total thermal radiation and values for the spark temperatures and radii were tabulated and graphed as functions of time for three explosions under three different sets of conditions. Total thermal radiation was obtained by graphically integrating the rate of thermal radiation over the time of the process. For two of the three explosions approximately 30 percent of the spark energy was emitted as thermal radiation. It was not possible to determine this fraction for the third explosion.

Analysis of the propagation of error shows that the error in the results for total thermal radiation is less than 7.5 times any error in the measurements of the radiation incident on the photoelectric tubes.

SUMMARY

Problem

The energy of an underwater spark is dissipated in the shock wave, in thermal radiation (light energy) and thermal conduction, and in the steam bubble. The energy from an underwater nuclear explosion is dissipated via the same pathways. The energy partition among these pathways is uncertain. If measurements of the total thermal radiation emitted by an underwater spark could be made, the values obtained may then be useful in experiments with miniature models of underwater nuclear explosions. They could also be compared with the estimates of the radiant energy emission from actual underwater nuclear explosions.

Findings

Values for the spark temperature, its radius and its rate of radiant energy emission were found as functions of time. From these the total thermal radiation was determined. It was found that about 30 percent of the spark energy was emitted as thermal radiation.

INTRODUCTION

To investigate the possibilities of simulating certain aspects of an underwater nuclear explosion with a miniature explosion, NRDL is studying some of the processes occurring when a wire is electrically exploded underwater. A major problem in the study of the exploding wire is to determine the explosion energy partition among the resultant shock wave, steam bubble and electromagnetic radiation. This report is devoted specifically to the determination of the total thermal radiant energy emitted during the brief, brilliant flash of the explosion.

The experimental approach to this problem is the conventional one where radiation from the explosion is measured at two wavelengths as a function of time with calibrated photoelectric tubes. A value for the total thermal radiant energy can then be computed using Planck's law for radiation from a black body source. Two questions arise at this point: (1) Is the system radiating with a Planckian distribution? (2) Is the method of analysis so sensitive to errors in the measurements that irreducible experimental error causes a prohibitively large error in the final solution?

Substantial evidence is given by Martin (Ref. 1) in favor of the system's radiating as a black body. He demonstrated theoretically that the underwater spark can be considered as progressing continuously through successive states of thermal equilibrium so that photons incident on this spark surface are distributed in Planckian manner. Martin further offered experimental evidence that the spark surface radiates like a black body in the visible region of the spectrum. Since light measurements in the present experiment are made in the visible region of the spectrum it seems justifiable, at least for the purposes of this experiment, to treat the spark as a black body.

The second question is investigated in Section IV. It is shown that the error in the value obtained for the total radiant energy emitted is less than 7.5 times any error incurred in the measurement of the experimental parameters. It is felt that this is surprisingly small and that the approach outlined above is feasible.

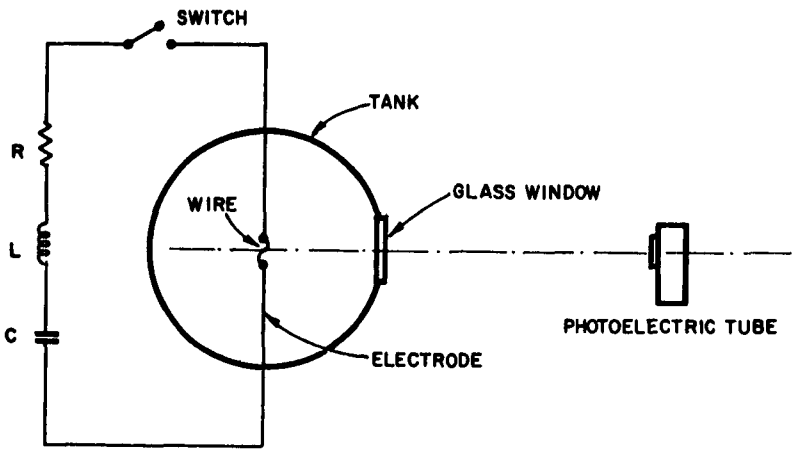

Fig. 1 Schematic Diagram of the Wire-exploding Facility

The underwater spark is produced in an indoor, water-filled tank, with a copper wire stretched between two centrally located electrodes (Fig. 1). Electrical energy is switched from a charged capacitor bank into the circuit containing the wire. The charged capacitor and attendent circuitry which includes the wire is an LCR system. When the switch is closed, the resultant current is a damped sinusoidal wave (Fig. 2). The wire is vaporized and a conducting plasma of copper atoms and water molecule fragments is formed. The shape of this plasma has been shown by photographic methods to be cylindrical with the axis of the cylinder defined by the wire.[2] The plasma is called the spark channel and the radiation is emitted from the spark channel surface. The resistance of the spark channel comprises approximately 40 % of the total resistance of the circuit so that about 40 % of the energy originally stored in the capacitor is dissipated through the spark channel.[3]

METHOD OF ANALYSIS AND WORKING EQUATIONS

The detailed method of analysis used to determine the total thermal radiant energy emitted at the spark channel surface is given below. First the determination of the channel temperature is discussed both from theoretical and experimental points of view. The Stefan-Boltzmann law is then introduced to give the rate of energy radiation per unit

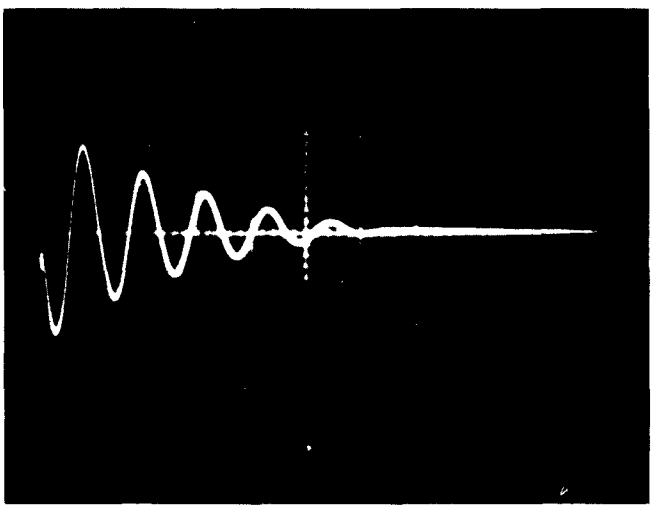

Fig. 2 Oscillograph of a Typical Channel Current
Gap = 1 inch; stored energy = 1800 j
Oscilloscope vertical sensitivity = 1 v/cm
Oscilloscope horizontal sensitivity = 20 μsec/cm

area of channel surface. The method of determining the total channel surface area is treated, and the equations for the rate of thermal radiation from the entire spark channel surface is derived. Finally, the working equations are presented by substituting known or measured values for the constants. The total thermal energy radiated during the whole process is obtained upon graphical integration of the rate of energy emission.

Spark Channel Temperature

The determination of the temperature of a black body from values for the radiation emitted at two different wavelengths is the basis of the experimental method used. Planck's law for black body radiation requires that J_λ, the radiation emitted at wavelength λ per unit time, per unit surface area, per unit wavelength, be

$$J_\lambda = 2 \pi hc^2 \lambda^{-5} \left(e^{\frac{hc}{\lambda kT}} - 1\right)^{-1}$$

where h = Planck's constant
c = speed of light
λ = wavelength of the radiation
k = Boltzmann's constant
T = black body temperature in degrees Kelvin

The ratio of two J_λ's defines a unique temperature for a black body.

If the temperature of a black body is varying in time, then measurement of the J_λ's for two wavelengths as functions of time defines the time function of the temperature. It is by these means that the time function of the spark channel temperature is determined.

The ratio $J_{\lambda_1}/J_{\lambda_2}$ is denoted by the symbol B. Solving the equation

$$B = \frac{J_{\lambda_1}}{J_{\lambda_2}} = \frac{\lambda_1^{-5}\left(e^{\frac{hc}{\lambda_1 kT}} - 1\right)^{-1}}{\lambda_2^{-5}\left(e^{\frac{hc}{\lambda_2 kT}} - 1\right)^{-1}}$$

for T gives the spark channel temperature.

The actual measurement of the radiation at a given wavelength is made by a photoelectric tube which has a Farrand interference filter covering the cathode to absorb all light except the narrow band at the desired wavelength. The photoelectric tube is calibrated so that the absolute value of the radiant flux incident on the cathode can be read directly from the voltage generated by the tube. The voltages are recorded on an oscillograph over the time of the emission process.

The relationship between J_λ, the radiation emitted at the spark channel surface, and E_λ, the radiant flux incident on the photoelectric tube cathode, can be written as follows:

$$E_\lambda = \frac{2\,RL\,J_\lambda \gamma_\lambda}{\pi\,D^2}$$

where R is the spark channel radius, L is the channel length, and D is the distance from the spark channel to the photoelectric tube. The tube must be aligned so that it sights along the perpendicular bisector of the spark channel axis (Fig. 3) and D must be much greater than R. The factor 2 RL in the numerator is the cross-sectional area of the channel which is seen by the tube cathode. The symbol γ_λ is the attenuation factor of the media between the spark channel and the photoelectric tube for radiation at wavelength λ.

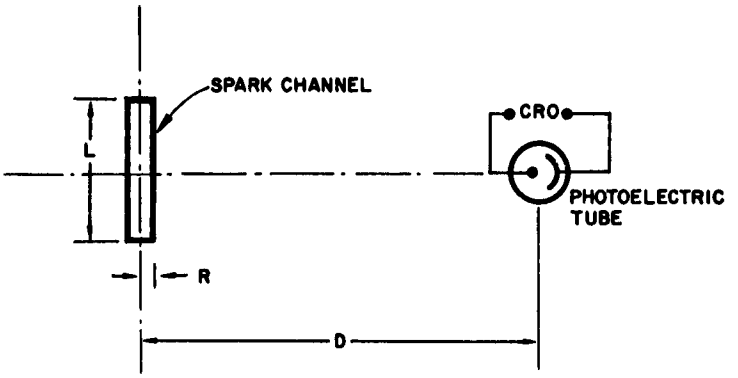

Fig. 3 Arrangement for Photoelectric Tubes and Spark Channel

The value of γ_λ is always a number less than one except when a perfect vacuum exists between the channel and the tube. It is assumed that the attenuation in air is insignificant for the distance involved so that γ_λ need be determined only for the water and glass in the explosion tank. A value for γ_λ is obtained by measuring the flux of wavelength λ incident on the photoelectric tube from a light source placed at the position of the wire in the tank, first with the tank empty and the glass window open, and then with the tank full and the window closed. The ratio of the latter measurement to the former is γ_λ.

B, the number which defines the spark channel temperature, can now be found in terms of the experimental parameters, E_λ and γ_λ, as follows:

$$\frac{E_{\lambda_1}}{E_{\lambda_2}} = \frac{\dfrac{2\,RL\,\gamma_{\lambda_1}\,J_{\lambda_1}}{\pi\,D^2}}{\dfrac{2\,RL\,\gamma_{\lambda_2}\,J_{\lambda_2}}{\pi\,D^2}} = \frac{\gamma_{\lambda_1}\,J_{\lambda_1}}{\gamma_{\lambda_2}\,J_{\lambda_2}}$$

This expression is true only when both photoelectric tubes (one for measuring the radiation at each wavelength) are properly aligned at the same distance from the spark channel. Then,

$$B = \frac{J_{\lambda_1}}{J_{\lambda_2}} = \frac{\gamma_{\lambda_2} E_{\lambda_1}}{\gamma_{\lambda_1} E_{\lambda_2}}$$

Total Thermal Radiant Energy

Once T is computed from B, the rate at which energy is radiated per unit area from the channel surface for all wavelengths is given by the Stefan-Boltzmann law. Where

$$W = \sigma T^4$$

and

σ = the Stefan-Boltzmann constant

W multiplied by the channel surface area, A_c, gives P, the rate of energy radiation for the entire channel surface.

A_c can be found from the equation,

$$E_\lambda = \frac{2\ RL\ J_\lambda\ \gamma_\lambda}{\pi\ D^2}$$

in the following manner:

$$A_c = 2\ \pi\ RL$$

$$\pi\ E_\lambda = (2\ \pi\ RL)\ \frac{J_\lambda\ \gamma_\lambda}{\pi\ D^2}$$

$$A_c = \frac{\pi^2\ D^2\ E_\lambda}{J_\lambda\ \gamma_\lambda}$$

Substituting

$$2\ \pi\ hc^2\lambda^{-5}\ (e^{hc/\lambda kT} - 1)^{-1}$$

for J_λ gives

$$A_c = \frac{\pi\ D^2\ \lambda 5\ E_\lambda}{2\ hc^2\ \gamma_\lambda}\ (e^{hc/\lambda kT} - 1)$$

Then P, the rate at which energy is radiated from the entire spark channel surface is:

$$P = \frac{\sigma \pi}{\gamma_\lambda} \quad \frac{D^2 \lambda^5 E_\lambda}{2 hc^2} \quad (e^{hc/\lambda kT} - 1) \, T^4.$$

The total radiant energy emitted by the channel is the integral of P dt taken over the entire explosion process. This integral is evaluated graphically by computing enough values for P to describe a curve of P versus time and then determining the area under the curve with the planimeter.

The Working Equations

By using predetermined values for the calibration constants and the load resistances of the photoelectric tubes, and by substituting numbers for the physical constants, the equations can be written in the working form actually used in reducing the experimental data to useful information.

The current i_λ developed in the photoelectric tube due to radiant flux E_λ incident on the cathode is related to E_λ by the equation $i_\lambda = \eta_\lambda E_\lambda$ where η_λ is the calibration constant. The voltage V_λ, across the load resistance, R_λ, is $R_\lambda i_\lambda$ and is recorded on the oscillograph. The ratio, B, then, can be written in terms of the voltages recorded as

$$B = \frac{\gamma_{\lambda_2} E_{\lambda_1}}{\gamma_{\lambda_1} E_{\lambda_2}} = \frac{R_{\lambda_2} \eta_{\lambda_2}}{R_{\lambda_1} \eta_{\lambda_1}} \cdot \frac{\gamma_{\lambda_2} V_1}{\gamma_{\lambda_1} V_2}$$

Using the values for the R's and η's which are given in the section "Instrumentation."

$$B = 0.424 \frac{\gamma_{\lambda_2} V_{\lambda_1}}{\gamma_{\lambda_1} V_{\lambda_2}}$$

where λ_1 is 407 mμ and λ_2 is 610 mμ in all cases in this report. To facilitate the calculation of the temperature, T, from a value for B, a standard curve of B versus T is graphed, using the equation

$$B = \frac{\lambda_2^5 \left(e^{hc/\lambda_2 kT} - 1\right)}{\lambda_1^5 \left(e^{hc/\lambda_1 kT} - 1\right)}$$

This graph is shown in Fig. 4.

The equation for the rate at which energy is radiated from the spark channel surface,

$$P = \frac{\pi \sigma D^2 \lambda^5 E_\lambda}{2 hc^2 \gamma_\lambda} \left(e^{hc/\lambda kT} - 1\right) T^4$$

can be evaluated using the data for either wavelength, 407 mμ or 610 mμ. In theory both sets of data should give the same value for P. In practice, however, the values are not exactly the same so that both are evaluated and their average value, $\bar{P} = (P_{407} + P_{610})/2$, is used to graph the relationship P versus time.

The working equations for P_{407} and P_{610} are

$$P_{407} = 0.882 \times 10^{-13} \frac{D^2}{\gamma_{407}} V_{407} \left(e^{3.54 \times 10^4/T} - 1\right) T^4 \text{ ergs/sec}$$

$$P_{610} = 1.57 \times 10^{-12} \frac{D^2}{\gamma_{610}} V_{610} \left(e^{2.36 \times 10^4/T} - 1\right) T^4 \text{ ergs/sec}$$

where D, the distance from the spark channel to the photoelectric tube, is in centimeters and V_λ, the voltage on the oscillograph, is millivolts.

The spark channel radius can be computed from the equation

$$\bar{P} = A_c \sigma T^4$$

as follows:

$$A_c = 2 \pi RL = \frac{P}{\sigma T^4}$$

$$R = \frac{P}{2 \pi L \sigma T^4}$$

$$R = \frac{2.8 \times 10^{-3} \bar{P}}{L T^4} \text{ centimeters}$$

where $\bar{P}$ is in ergs per second and L is in centimeters.

The quantities described above are tabulated and graphed in Section V for 3 explosions under 3 different sets of conditions.

INSTRUMENTATION

The photoelectric tubes used for making the radiation measurements at 407 and 610 mμ are the RCA 929 and 925 tubes respectively. The 407 and 610 mμ Farrand interference filters have peak transmissions of 31 percent and 23 percent and half bandwidths of 17 mμ and 13 mμ respectively. In addition to the interference filter, a neutral filter is used with the 929 photoelectric tube in order to keep the tube current below levels at which saturation might occur. The neutral filter has a transmission of approximately 5 percent at 407 mμ.

Figure 5 is a schematic diagram of the photoelectric tube circuits. Each tube is powered by a 300 volt dry cell battery which has a 0.101 μf capacitor across its terminals to insure against a momentary loss of voltage in the case of large currents in the photoelectric tube circuits. Load resistances of 532 ohms, 2.21 kilohms, 21.4 kilohms, 215 kilohms and 2 megaohms are available in the circuit for the tube measuring radiation at 407 mμ. For the other, load resistances of 535 ohms, 2.23 kilohms, 20.5 kilohms, 210 kilohms,and 2 megohms can be selected. The voltages generated across the load resistances are measured on a single Tektronix dual beam type 551 oscilloscope with two type K fast-rise-time preamplifiers. During calibration and during the determination of the γ_λ's, the more sensitive type D pre-amplifiers are used, because the radiation intensities are much lower.

Each photoelectric tube with its circuit components is shielded electrostatically in an aluminum box in which the window is covered by the filter. The boxes are carefully sealed against all light except that entering through the filter.

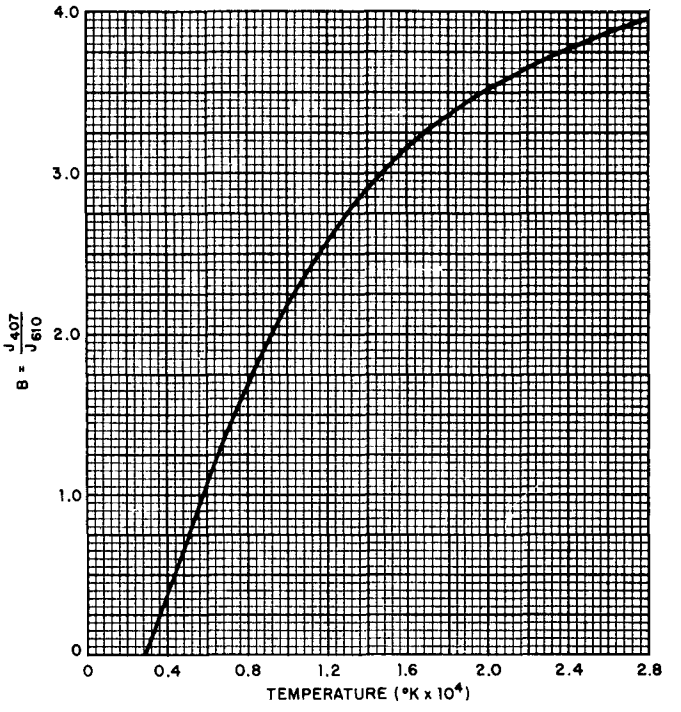

Fig. 4 Ratio B of Flux Intensities at Wavelengths 707 and 610 mμ from a Black Body

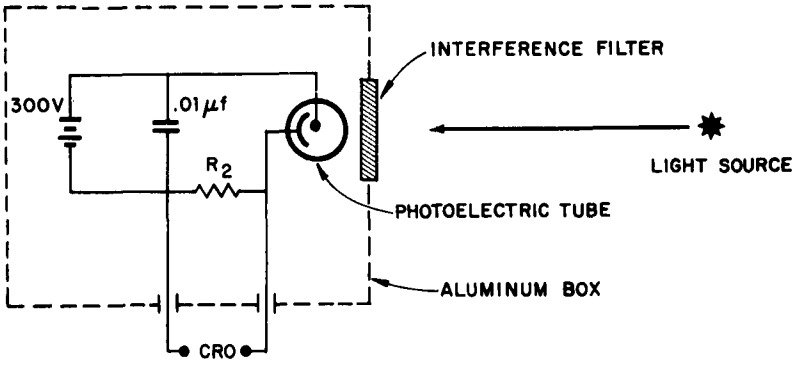

Fig. 5 Schematic Diagram of Photoelectric Tube Circuitry

Each filter-photoelectric tube unit is calibrated to give radiant flux in direct proportion to the current flowing through the load resistance. Once calibration is accomplished the only component which can be altered in the unit is the load resistance.

Two independent methods of calibration are used and the results averaged. One method employs a standard lamp which emits light with a flux density at 25 cm from the envelope of 1.6 $\mu w\ (cm^2 \cdot m\mu)^{-1}$ at 407 $m\mu$, and 13.1 $\mu w\ (cm^2 \cdot m\mu)^{-1}$ at 610 $m\mu$ when powered by 15.4 amps A.C. The values for flux densities are rms. The second method employs a G.E. type 18A-T10-2-6V lamp which has a rectangular tungsten filament with a surface area on one side of 0.144 cm^2. The apparent temperature of the filament is determined with an optical pyrometer and the true temperature is found using values for the spectral emissivity (ϵ_λ) of tungsten from Forsythe and Worthing.[4] The flux density at 407 and 610 $m\mu$, D cm from the filament on an axis normal to the plane of the filament at its center, is calculated from the equation

$$E_\lambda = \frac{\epsilon_\lambda J_\lambda A_f}{\pi D^2}$$

where A_f is the filament area and where J_λ is computed using Planck's law. The value for the true temperature, and the values for ϵ_λ are taken from Forsythe and Worthing. Since the flux density and the photoelectric tube current are related by the equation $i_\lambda = \eta_\lambda E_\lambda$, η_λ, the calibration constant for the filter-photoelectric tube unit measuring the radiation at wavelength λ, can be evaluated from the equation

$$\eta_\lambda = \frac{\pi D^2 i_\lambda}{\epsilon_\lambda J_\lambda A_f} = \frac{i_\lambda}{E_\lambda}$$

The two methods agreed within 7 percent and gave average values of

$$\eta_{407} = 0.0881\ \mu a \cdot cm^2 \cdot m\mu \cdot (\mu)^{-1},$$

$$\eta_{610} = 0.0392\ \mu a \cdot cm^2 \cdot m\mu \cdot (\mu)^{-1}.$$

In selecting the proper load resistances, there are two factors to consider. One is to have the load resistance great enough so that the stray pick-up detected by the photoelectric tube-oscilloscope circuitry,

that is due to the large currents in the exploding wire facility, is not significant compared to the voltage across the load resistance. The other is to have the RC time constant (load resistance multiplied by the input capacitance) small enough to make it certain that the oscilloscope is responding accurately to the light signals incident upon the photoelectric tube. The Tektronix type K pre-amplifiers with their low input capacitance of 20 μμf are used with only 22 inches of amphenol type RG-62A connecting cables. The tubes are placed close enough to the exploding wire that the photoelectron currents are as great as possible without reaching saturation levels. This requires that load resistances of about 20 kilohms be used. The actual values of the load resistances were determined with a Leeds and Northrup ohmmeter.

An attempt was made to determine how large a current the photoelectric tubes could carry for times of 100 microseconds before their responses became non-linear. Measurements of the light from identical explosions at progressively shorter distances from the spark channel were made. The currents recorded were up to 50 microamperes. No attempt was made to measure currents higher than 50 microamperes so that the actual saturation currents may have been considerably higher for those short times. Currents measured during actual data runs were below these values.

THE PROPAGATION OF ERROR

The precision with which experimental determinations are known depends upon two prime factors. First, the technical precision with which the experimental parameters are measured, and second, the manner in which any error in the measurement of the parameters is propagated via the mathematics used to develop the final expression.

The standard deviation of a number of determinations is one way of expressing precision, and it embodies the two factors mentioned above.

Since the number of determinations in the present experiment were limited no standard deviations could be found; only qualitative statements can be made about precision. These qualitative statements are based upon the good reproducibility of the experimentally measured parameters in the formative stages of the experiment, and upon the determination of an upper limit to the growth of the error in the E_λ's, as these parameters were mathematically converted into the expression for total energy radiated.

The determination of the upper limit to the growth in error is made according to Scarborough's method of propagation of error and is given below.

Scarborough[5] shows that the relative error in a function having several independent parameters

$$Q = Q\ (U_1,\ U_2,\ \ldots\ U_n)$$

is expressed by the relationship

$$E_r = \frac{\Delta Q}{Q} = \frac{1}{Q}\left(\frac{\partial Q}{\partial U_1}\ \Delta U_1 + \frac{\partial Q}{\partial U_2}\ \Delta U_2 + \ldots + \frac{\partial Q}{\partial U_n}\ \Delta U_n \right) .$$

The function of interest here is the integral, $\int Pdt$, the total thermal energy radiated. The relative error in this function can be evaluated in terms of the radiant fluxes, E_{407} and E_{610}, the attenuation factors, γ_{407} and γ_{610}, and the distance, D, from the spark channel to the photoelectric tubes. Thus,

$$Q = \int Pdt = Q\ (E_{407},\ E_{610},\ \gamma_{407},\ \gamma_{610},\ D)$$

and

$$E_r = \frac{\Delta Q}{Q} = \frac{\Delta \int Pdt}{\int Pdt} = \frac{1}{Q}\left(\frac{\partial Q}{\partial E_{407}}\ \Delta E_{407} + \ldots + \frac{\partial Q}{\partial D}\ \Delta D \right) .$$

It is clear that the relative error $\Delta \int Pdt / \int Pdt$ is always equal to or less than the maximum value of $\Delta P/P$ during the time of integration so that the maximum value of $\Delta P/P$ provides an upper limit to $\Delta \int Pdt / \int Pdt$. It is this function $(\Delta P/P)$ max. that will be evaluated.

Let $$P = P\ (E_{407},\ E_{610},\ \gamma_{407},\ \gamma_{610},\ D)$$

errors in E_{407} and E_{610} are assumed to be the only ones of significance. Then

$$\frac{\Delta P}{P} = \frac{1}{P}\left(\frac{\partial P}{\partial E_{407}}\ \Delta\ E_{407} + \frac{\partial P}{\partial E_{610}}\ \Delta\ E_{610} \right)$$

Since $P = \sigma A_c T^4$ where A_c is spark channel surface area and T is its temperature, then by partial differentiation

$$\frac{\Delta P}{P} = \frac{\Delta A_c}{A_c} + \frac{4\,\Delta T}{T} .$$

Expressing $\Delta A_c/A_c$ and $\Delta T/T$ in terms of $\Delta E_{407}/E_{407}$ and $\Delta E_{610}/E_{610}$ gives $\Delta P/P$ as a function of the significant relative errors in the experimental parameters.

Evaluation of $\Delta T/T$

Figure 4 gives the relationship between the temperature, T, and the experimentally determined number B. Any small variation in T is related to a variation in B by the equation

$$\Delta B = \frac{dB}{dT} \Delta\, T$$

where dB/dT is the slope of the curve B versus T in the region of the temperature variation. Multiplying by $1/T(dB/dT)^{-1}$ gives

$$\frac{\Delta T}{T} = \frac{1}{T}\left(\frac{dB}{dT}\right)^{-1} \Delta B.$$

But

$$B = \frac{\gamma_{610}}{\gamma_{407}} \frac{E_{407}}{E_{610}}$$

and the relative error in B is

$$\frac{\Delta B}{B} = \frac{\Delta E_{407}}{E_{407}} - \frac{\Delta E_{610}}{E_{610}} .$$

Assuming that positive and negative ΔE_λ's are equally likely and that

$$\frac{\Delta E_{407}}{E_{407}} = \frac{\Delta E_{610}}{E_{610}}$$

then

$$\frac{\Delta B}{B} \leq \frac{2\Delta\, E_\lambda}{E_\lambda}$$

and

$$\Delta B = 2\,B\,\frac{\Delta E_\lambda}{E_\lambda}$$

where either E_{407} or E_{610} may be used for E_λ.

Substituting this for ΔB in the equation for $\Delta T/T$ gives,

$$\frac{\Delta T}{T} \leq \frac{2B}{T}\,\frac{dB}{dT}^{-1}\,\frac{\Delta E_\lambda}{E_\lambda}\,.$$

Both B and dB/dT can be found using the graph of B versus T (Fig. 4).

Evaluation of $\Delta A_c/A_c$

It has been shown that

$$A_c = \frac{\pi\, D^2\, \lambda^5\, E_\lambda\, (e^{hc/\lambda kT}-1)}{2\, hc^2\, \gamma_\lambda}$$

The relative error in A_c due to errors in E_λ and T is also derived according to the method of Scarborough, and is

$$\frac{\Delta A_c}{A_c} = \frac{\Delta E_\lambda}{E_\lambda} - \frac{hc}{\lambda kT}\left(\frac{e^{hc/\lambda kT}}{e^{hc/\lambda kT}-1}\right)\frac{\Delta T}{T}$$

where $\Delta T/T$ is as above.

The expressions for $\Delta T/T$ and $\Delta A_c/A_c$ are now substituted into the original equation

$$\frac{\Delta P}{P} = \frac{\Delta A_c}{A_c} + \frac{4\,\Delta T}{T}$$

to yield

$$\frac{\Delta P}{P} \leq \left[1 + \frac{2B}{T} \left(\frac{dB}{dT} \right)^{-1} \left(4 - \frac{\frac{hc}{\lambda kT} e^{hc/\lambda kT}}{e^{hc/\lambda kT} - 1} \right) \right] \frac{\Delta E_\lambda}{E_\lambda}$$

A discussion of the evaluation of $\Delta P/P$ can be found in the next section.

RESULTS

Total Thermal Radiation

The radiation from three exploding wires was measured by the photoelectric tubes and recorded on oscillographs, and values for the spark channel temperatures, radiant powers, and radii were computed as functions of time. The times of radiation emission were about 100 microseconds. The total thermal energies radiated were determined graphically. The conditions are tabulated in Table 1. The computed quantities for

TABLE 1

Explosion Conditions

Explosion	V_o* (kv)	E_o** (joule)	L (cm)	D (cm)	γ_{407}	γ_{610}
1	25	1800	3.81	730	0.594	0.539
2	25	1300	2.54	730	0.563	0.500
3	15	648	2.54	457	0.526	0.561

* V_o = Initial voltage on capacitor.
** E_o = Energy initially stored in capacitor.

all three explosions are listed in Table 2. The oscillographs taken for the three explosions are shown in Fig. 6. Figures 7, 8, and 9 are graphs of the computed quantities over the times of the explosions.

TABLE 2

Computed Quantities From Three Explosions

Time (μsec.)	V_{407} (mV)	V_{610} (mV)	B	T_o (K)	P_{407} (erg/sec.)	P_{610} (erg/sec.)	$\bar{P}$ (erg/sec.)	R (cm)	E (joules)
					Explosion 1				
5	469	75	2.41	11.1×10^3	1.32×10^{13}	1.31×10^{13}	1.32×10^{13}	0.65	
10	857	116	2.83	13.6	2.87	2.82	2.85	0.64	
20	1230	165	2.87	13.9	4.31	4.28	4.30	0.87	
30	1330	176	2.89	14.0	4.71	4.66	4.69	0.90	
40	1250	175	2.75	13.1	4.13	4.08	4.11	1.03	
50	1095	164	2.58	12.0	3.28	3.27	3.28	1.17	
60	876	140	2.41	11.1	2.47	2.44	2.46	1.20	
70	719	113	2.46	11.4	2.08	2.07	2.08	0.91	
80	563	91	2.37	10.9	1.59	1.57	1.58	0.82	
90	438	65	2.60	12.2	1.35	1.34	1.35	0.45	
100	313	41	2.93	14.2	1.13	1.11	1.12	0.21	270
					Explosion 2				
5	420	58.5	2.69	12.7×10^3	1.41×10^{13}	1.40×10^{13}	1.41×10^{13}	0.59	
10	730	92.0	3.01	14.9	2.97	2.98	2.98	0.67	
20	1010	131	2.92	14.2	3.86	3.87	3.87	1.05	
30	1025	147	2.64	12.4	3.35	3.37	3.36	1.57	
50	780	125	2.36	10.9	2.31	2.32	2.32	1.80	
60	655	109	2.28	10.5	1.89	1.91	1.90	1.72	
70	505	84.5	2.26	10.4	1.44	1.45	1.45	1.37	
80	370	60.0	2.32	10.7	1.09	1.08	1.09	0.91	
90	280	43.0	2.46	11.4	0.85	0.85	0.85	0.56	
100	200	29.0	2.62	12.3	0.65	0.65	0.65	0.31	209
					Explosion 3				
5	98	47	0.94	5.7×10^3	0.22×10^{13}	0.22×10^{13}	0.22×10^{13}	1.90	
10	298	90	1.50	7.4	0.38	0.37	0.38	1.37	
20	570	141	1.83	8.5	0.66	0.65	0.66	1.39	
30	616	152	1.84	8.6	0.72	0.70	0.71	1.45	
40	552	137	1.82	8.5	0.64	0.62	0.63	1.37	
50	450	110	1.85	8.6	0.53	0.51	0.52	1.05	
60	348	83	1.90	8.8	0.40	0.40	0.40	0.74	
70	256	56	2.07	9.5	0.30	0.29	0.30	0.40	
80	162	32	2.29	10.5	0.20	0.20	0.20	0.18	
90	92	16	2.60	12.2	0.12	0.12	0.12	0.06	38.8
100									

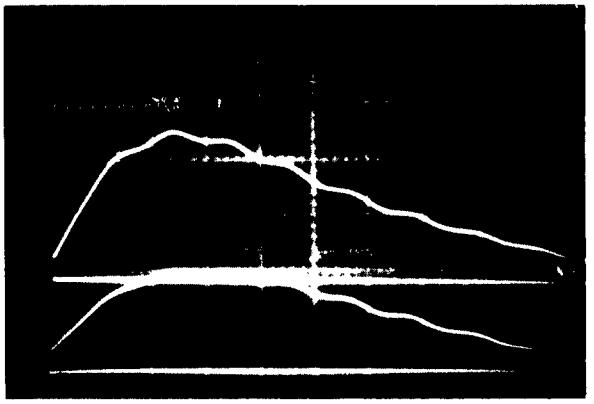

a. Explosion 1
Upper trace sensitivity = 0.5 V/cm
Lower trace sensitivity = 0.1 V/cm
Sweep speed = 10 μsec/cm

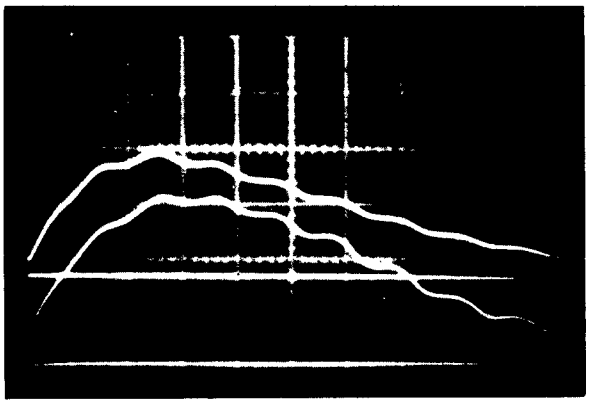

b. Explosion 2
Upper trace sensitivity = 0.5 V/cm
Lower trace sensitivity = 0.05 V/cm
Sweep speed = 10 μsec/cm

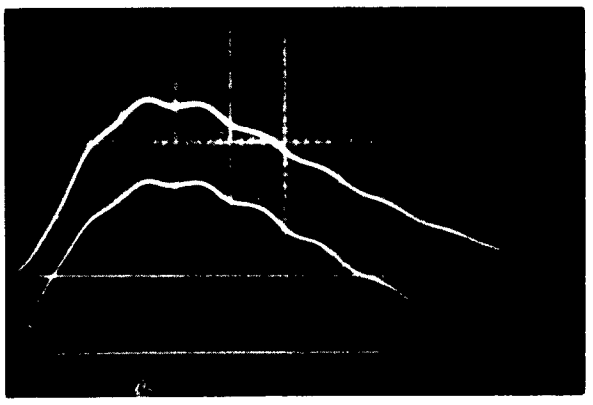

c. Explosion 3
Upper trace sensitivity = 0.2 V/cm
Lower trace sensitivity = 0.05 V/cm
Sweep speed = 10 μsec/cm

Fig. 6 Oscillographs of the Radiation Intensities
Upper trace measures radiation at 407 mμ
Lower trace measures radiation at 610 mμ

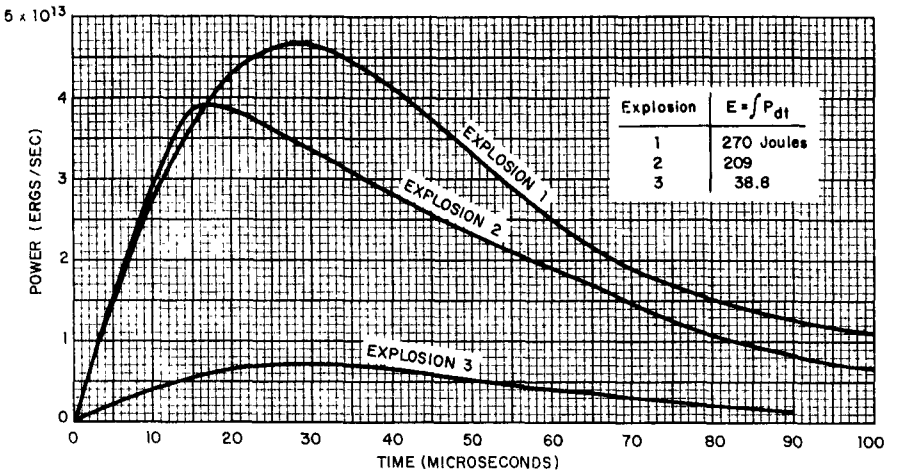

Fig. 7 Rate of Energy Radiation from the Spark Channel Surface for Three Explosions

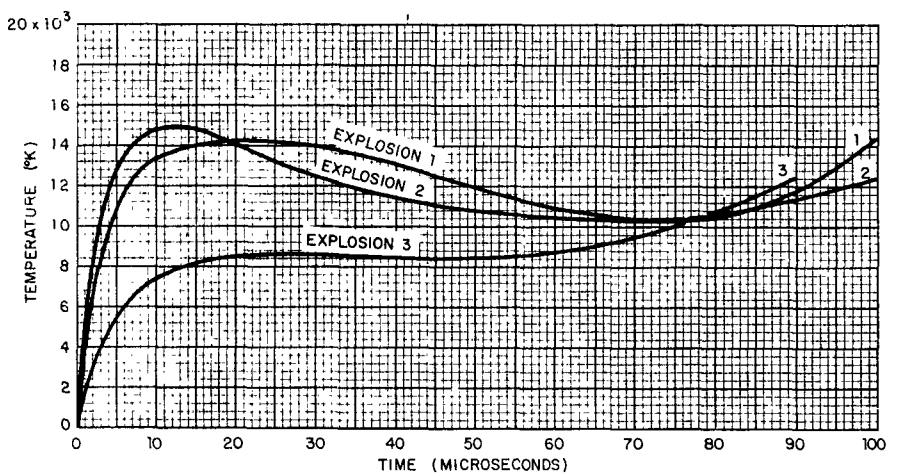

Fig. 8 Spark Channel Temperature for Three Explosions

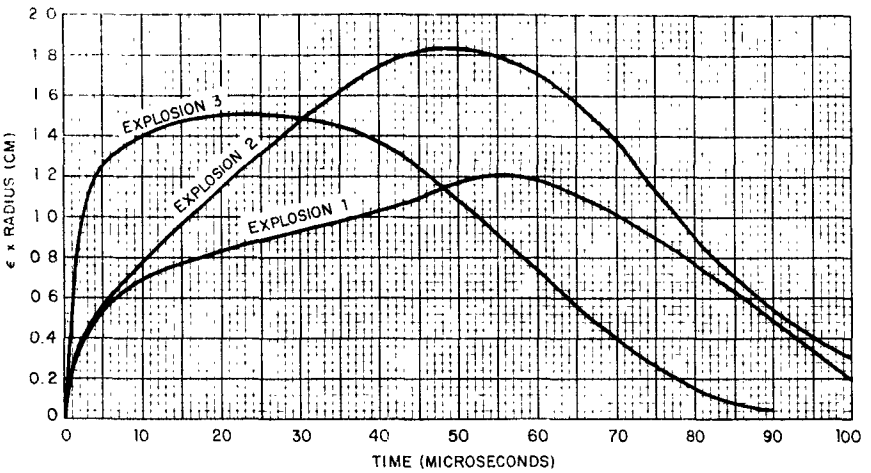

Fig. 9 Spark Channel Radius for Three Explosions

Two of the explosions were made with the 5.76-μf capacitor initially charged to 25 kv, one with a gap (wire length) of 1-1/2 inches and the other with a gap of 1 inch. The energy initially stored in the capacitor in these two cases was 1800 joules. For the third explosion, the capacitor was charged to 15 kv and the gap was 1 inch. The initially stored energy was 648 joules.

In all cases the wire was 5 mil copper, the depth of the gap below the surface of the water was 6 inches, the pressure over the water was ambient, and the water temperature was approximately 75°F.

Evaluation of Error

The results show that the majority of the radiation occurs when T is between 4000 and 15,000°K. In this region $\Delta P/P$ is a maximum when T is in the neighborhood of 15,000°K. Evaluation $\Delta P/P$ when $\lambda = 610$ mμ gives

$$\frac{\Delta P}{P} \leq 0.75 \frac{\Delta E_{610}}{E_{610}}$$

The relative error in the total energy radiated is then less than 7.5 times any error in the measurements of the radiant fluxes. Further it is estimated that these errors in measurement are less than 10 percent.

DISCUSSION

The total radiant energies emitted were 15.0, 11.6 and 5.96 percent, respectively for explosions 1, 2, and 3, of the energies initially stored in the capacitors. These percentages are derived from the values listed in Tables 1 and 2. Buntzen, with the apparatus used in the present experiment, determined that 42 percent of the initially stored energy is put into the spark channel when the conditions of explosion 2 exist. Thus, the energy thermally radiated in explosion 2 was 11.6/0.42 or 27.6 percent of the total energy dissipated by the spark channel, the remaining 72.4 percent going into the shock wave, the bubble and into thermal conduction.

Explosion 1 differed from explosion 2 only in that the spark channel was 1-1/2 times longer. Assuming that the resistance of the spark channel varies directly with its length, it can be shown that if 42 percent of the stored energy went into the spark channel in explosion 2, then 51 percent must have gone into the spark channel in explosion 1. Then the thermal radiation was 15/0.51 or 29 percent of the total spark channel energy. For explosions 1 and 2, roughly 30 % of the energy put into the spark channel was later emitted as radiant energy.

The conditions of explosion 3 were identical to those of explosion 2, except that in the former the energy initially stored in the capacitors was only one third of what it was in the latter. The total spark channel energy was unknown and presently no explanation can be offered for the comparatively low yield of radiant energy.

Some apparent discrepancies in the experiment are indicated by the values obtained for the spark channel temperatures and radii. These show the temperatures increasing and the radii decreasing at times late in the emission process. It is known that the energy input to the spark channel has fallen to relatively low values at these times (see Fig. 2) so it seems that the channel temperature should be decreasing. Further, there is no reason for the channel radius to decrease at a time when the pressures within are still very high as indicated by Martin's work.[1]

To best evaluate these discrepancies it is important to note how error in T^4 and error in A_c contribute to this error in $\sigma A_c T^4$ or P. The final expression for $\Delta P/P$ in the section "The Propagation of Error" contains the factor

$$4 - \left(\frac{hc}{\lambda kT} e^{hc/\lambda kT}\right)\left(e^{hc/\lambda kT} - 1\right)^{-1}$$

It can be seen that the number 4 is from the above expression for the error in T^4 while

$$\left(\frac{hc}{\lambda kT} e^{hc/\lambda kT}\right)\left(e^{hc/\lambda kT} - 1\right)^{-1}$$

is from the expression for the error in A_c. These two quantities are opposite in sign, and, at 15,000°K, close to being equal in magnitude. Therefore the relative error $\Delta P/P$ is less than the relative error in either T^4 or A_c, and the confidence with which the values for the total radiated energy can be accepted is greater than for either the values for T^4 or for the values for the radii which are directly proportional to A_c.

Further investigation should be directed toward the explanation of the results for the temperatures and radii. Also the emissivities of the spark showed surface should be determined over as wide a wavelength spectrum as possible so that it can be known more precisely how closely the spark resembles a black body.

BIBLIOGRAPHY

1. E. A. Martin. The Underwater Spark: An Example of Gaseous Conduction at About 10,000 Atmospheres. Engineering Research Institute: Ann Arbor, Michigan, July 1957.

2. W. G. Chace, H. K. Moore. Exploding Wires. Plenum Press, Inc., New York. Chapman and Hall, Ltd., London, 1959.

3. R. R. Buntzen. "The Use of Exploding Wires in the Study of Small Scale Underwater Explosions". To be published in A Symposium on Exploding Wires, by Plenum Press, Inc., New York.

4. W. E. Forsythe, A. G. Worthing. "The Properties of Tungsten and the Characteristics of Tungsten Lamps". Astrophysical Jour. 61, 141 (1925).

5. J. B. Scarborough. Numerical Mathematical Analysis. The Johns Hopkins Press, Baltimore, 1950.

INITIAL DISTRIBUTION

Copies	NAVY
3	Chief, Bureau of Ships (Code 335)
1	Chief, Bureau of Ships (Code 320)
1	Chief, Bureau of Ships (Code 423)
1	Chief, Bureau of Ships (Code 362B)
1	Chief, Bureau of Medicine and Surgery
2	Chief, Bureau of Naval Weapons
1	Chief, Bureau of Naval Weapons (RRMA-11)
1	Chief, Bureau of Naval Weapons (RRE-5)
1	Chief, Bureau of Naval Weapons (SP-2721)
2	Chief, Bureau of Yards and Docks (Code 74)
1	Chief, Bureau of Yards and Docks (Code C-400)
1	Chief of Naval Operations (Op-07T)
1	Chief of Naval Operations (Op-446)
1	Chief of Naval Operations (Op-03EG)
1	Chief of Naval Operations (Op-75)
1	Chief of Naval Operations (Op-91)
1	Chief of Naval Operations (Op-922G2)
1	Chief of Naval Research (Code 104)
1	Chief of Naval Research (Code 418)
1	Chief of Naval Research (Code 811)
1	Commander, New York Naval Shipyard (Material Lab.)
3	Director, Naval Research Laboratory (Code 2021)
2	Director, Naval Research Laboratory (Code 6370)
1	Office of Naval Research (Code 422)
1	CO, U.S. Naval Civil Engineering Laboratory
1	U.S. Naval School (CEC Officers)
1	Commander, Naval Air Material Center, Philadelphia
1	CO, Naval Air Development Center
1	CO, Naval Medical Research Institute
1	U.S. Naval Postgraduate School, Monterey
1	Commander, Naval Ordnance Laboratory (Library)
1	Commander, Naval Ordnance Laboratory (EU)
1	Commander, Naval Ordnance Laboratory (E)
1	Commander, Naval Ordnance Laboratory (EA)
1	CO, Navy Electronics Laboratory
1	CO, Navy Electronics Laboratory (Code 2350)
1	CO, Navy Electronics Laboratory (Code 2632C)

1	Commander, Naval Ordnance Test Station, China Lake
1	Commander, Naval Ordnance Test Station, Pasadena
1	Director, Naval Weapons Laboratory, Dahlgren
1	CO, Naval Schools Command, Treasure Island
1	CO, Naval Damage Control Training Center, Philadelphia
1	Naval Air Special Weapons Facility, Kirtland
1	CO, Nuclear Weapons Training Center, Pacific
1	CO, Nuclear Weapons Training Center, Atlantic
1	CO, David Taylor Model Basin (Library)
1	CO, David Taylor Model Basin (Code 700)
1	CO, David Taylor Model Basin (Code 775)
1	CO, Navid Taylor Model Basin (Code 780)
1	Office of Patent Counsel, San Diego
1	CO, Naval Supply Research and Development Facility
1	Superintendent, U.S. Naval Academy
1	President, Naval War College
1	Director, Institute of Naval Studies
1	CO, Naval Air Development Squadron 5, VX-5
2	Commandant of the Marine Corps (AO3H)
1	Commandant, Marine Corps Schools, Quantico (CMCLFDA)
1	Director, Landing Force Development Center
1	Commander, Operational Test and Evaluation Force, Atlantic
1	Commander, Operational Test and Evaluation Force, Pacific
1	Commander, Western Sea Frontier
1	Commandant, U.S. Coast Guard (OIN)

ARMY

1	Deputy Chief of Staff for Military Operations
1	Deputy Chief of Staff, Intelligence
1	Chief of Research and Development (Atomic Div.)
1	Chief of Research and Development (Life Science Div.)
1	Deputy Chief of Staff for Military Operations (DGM)
1	Deputy Chief of Staff for Military Operations (CBR)
1	Chief of Engineers (ENGMC-EB)
1	Chief of Engineers (ENGTB)
1	Chief of Engineers (ENGMC-DE)
1	Chief of Engineers (ENGCW)
1	CG, Army Materiel Command (AMCRD-DE-NE)
1	CG, Ballistic Research Laboratories
2	CG, USA CBR Agency
3	CO, BW Laboratories
1	CO, Fort McClellan, Alabama
1	Superintendent, U.S. Military Academy
1	Commandant, Guided Missile School, Redstone Arsenal
1	Commandant, Army Ordnance School, Aberdeen
1	Commandant, Quartermaster School, Fort Lee
1	Commandant, Infantry School, Fort Benning
1	Commandant, Chemical Corps Schools, Fort McClellan
1	CG, CBR Combat Developments Agency
1	CG, Army Combat Surveillance Agency

1	CO, Chemical Research and Development Laboratories
1	Commander, Chemical Corps Nuclear Defense Laboratory
1	CG, Aberdeen Proving Ground
1	CO, Army Medical Research Laboratory
1	CG, Medical Service School, Fort Sam Houston (Stimson Lib)
1	Director, Walter Reed Army Medical Center
1	CG, Combat Developments Command (CDCMR-V)
1	CG, Quartermaster Res. and Eng. Command
1	Hq., Dugway Proving Ground
3	The Surgeon General (MEDNE)
1	CO, Army Research and Development Laboratory
1	CO, Army Research and Development Laboratory (Evans Area)
1	CO, Army Signal School, Fort Monmouth
1	CG, Army Electronic Proving Ground
1	Combat Development Experimentation Center, Fort Ord
3	CG, Combat Development Command
1	CG, The Engineer Center, Fort Belvoir
1	CG, Engineer Res. and Dev. Laboratory
1	Commandant, Army Transportation School, Fort Eustis
1	CO, Transportation Combat Developments Agency
1	CO, Transportation Research Command
1	Commandant, Army Artillery and Missile School, Fort Sill
1	Commandant, Army Armored School, Fort Knox
1	Commandant, Air Defense School, Fort Bliss
1	Commandant, Army Aviation School, Fort Rucker
1	President, Army Aviation Board, Fort Rucker
1	President, Army Air Defense Board, Fort Bliss
1	President, Army Infantry Board, Fort Benning
1	President, Army Artillery Board, Fort Sill
1	Director, Office of Special Weapons Development
1	Director, Waterways Experiment Station
1	CO, Diamond Ordnance Fuze Laboratories (Code 230)
1	CG, Munitions Command
1	CO, Watertown Arsenal
1	CG, Army Missile Command
1	CO, 9th Hospital Center, Europe
1	Commandant, Command and General Staff College
1	Commandant, Army War College

AIR FORCE

1	Deputy Chief of Staff, Operations (Operations Analysis)
1	Director of Research and Development, DCS/D
2	Assistant Chief of Staff, Intelligence (AFCIN-3A2A)
1	Deputy Chief of Staff, Operations (AFOOP)
1	Assistant Chief of Staff, Intelligence, USAFE
6	CG, Aeronautical Systems Division (ASAPRDONS)
1	CG, Air Force Systems Command (RDRWA)
1	Directorate of Civil Engineering (AFOCE)
2	Director, USAF Project RAND

1	Director, USAF Project RAND (Dr. Rapp)
1	Commandant, School of Aerospace Medicine, Brooks AFB
1	CG, Strategic Air Command (OAWS)
1	Office of the Surgeon (SUP3.1), Strategic Air Command
1	Office of the Surgeon General
2	CG, Special Weapons Center, Kirtland AFB
1	Director, Air University Library, Maxwell AFB
1	Commander, 3415th M&SG
1	Commander, Electronic Systems Division (CRZT)
1	Air Force Cambridge Research Laboratory (CRQST-2)
1	CiC, Air Defense Command (ADLDC-A)
1	Commander, Tactical Air Command
1	Commander, Alaskan Air Command (AAOTN)
1	CiC, Pacific Air Forces (PFCIE-MB)
1	Air Force Technical Applications Center (Scheid)
1	Commander, Western Development Division (WDSIT)
1	Commander, 1009th Special Weapons Squadron

OTHER DOD ACTIVITIES

6	Chief, Defense Atomic Support Agency (Library)
1	Chief, Defense Atomic Support Agency (Vickery)
6	Commander, Field Command, DASA, Sandia Base
1	Commander, Field Command, DASA, Sandia Base (FCDV)
1	Commander, Field Command, DASA, Sandia Base (FCTG)
3	Commander, Field Command, DASA, Sandia Base (FCWT)
1	Commander, Field Command, DASA, Sandia Base (FCTG5, Library)
2	Office of Civil Defense, Washington
1	Office of Civil Defense, Washington (Miller)
2	Civil Defense Unit, Army Library
1	Director of Defense Research and Engineering
1	Director, Armed Forces Institute of Pathology
1	Commandant, Armed Forces Staff College
1	Commandant, Industrial College of the Armed Forces
20	Armed Services Technical Information Agency
1	Director, Armed Forces Radiobiology Research Institute
1	Director, Advance Research Projects Agency
1	Director, Weapons Systems Evaluation Group
1	Commander, JTF-8

AEC ACTIVITIES AND OTHERS

1	Research Analysis Corporation
2	Albuquerque Operations Office
1	Argonne National Laboratory
1	AEC Scientific Representative, France
1	AEC Scientific Representative, Japan
3	Atomic Energy Commission, Washington (Library)
1	Atomic Energy Commission, Washington (Corsbie, DBM)
1	Atomic Energy Commission, Washington (Starbird, DMA)

1	Atomic Energy Commission, Washington (Hooper)
1	Atomic Energy Commission, Washington (Joseph)
1	Atomic Energy Commission, Washington (Hollister)
5	Atomic Energy of Canada, Limited
2	Atomics International
1	Battelle Memorial Institute
2	Beers, Roland F., Inc.
1	Brookhaven National Laboratory
1	Bureau of Mines, College Park
1	Bureau of Mines, Laramie
1	Bureau of Mines, Washington
1	California Institute of Technology, Pasadena
1	Carnegie Institution
1	Division of Peaceful Nuclear Explosives, Washington
1	Division of Raw Materials, Washington
1	duPont Company, Aiken
1	duPont Company, Wilmington
1	Fundamental Methods Association
1	General Atomic Division
1	General Electric Company, Cincinnati
1	General Electric Company, Richland
1	General Electric Company, San Jose
1	Grand Junction Office
1	Harvey Mudd College
1	Hawaii Marine Laboratory
1	Holmes and Narver, Inc.
1	Homestake Mining Company
1	Johns Hopkins University (Wolman)
1	Knolls Atomic Power Laboratory
1	Lamont Geophysical Laboratory
2	Los Alamos Scientific Laboratory (Library)
1	Lovelace Clinic
1	Michigan State University (Triffett)
1	Moran, Proctor, Mueser and Rutledge
1	Mound Laboratory
2	NASA, Scientific and Technical Information Facility
2	Nevada Operations Office
1	Office of Assistant General Counsel for Patents
1	Phillips Petroleum Company
1	Power Reactor Development Company
1	Public Health Service, Washington
1	Reynolds Electrical and Engineering Company, Inc.
1	Sandia Corporation, Albuquerque (Library)
1	Sandia Corporation, Albuquerque (Merritt)
1	Sandia Corporation, Albuquerque (Reed)
1	Sandia Corporation, Livermore
5	San Francisco Operations Office
1	Scripps Institution of Oceanography (Van Dorn)
1	Scripps Institution of Oceanography (Folsom)
1	Space Technology Laboratories, Inc.
1	State of California, Department of Fish and Game (Bissell)

1	Tennessee Valley Authority
1	Tracerlab, Inc., Richmond
1	Union Carbide Nuclear Company (ORGDP)
4	Union Carbide Nuclear Company (ORNL)
1	U.S. Coast and Geodetic Survey, San Francisco
3	U.S. Coast and Geodetic Survey, Washington
1	U.S. Geological Survey, Albuquerque
1	U.S. Geological Survey, Denver
1	U.S. Geological Survey, Menlo Park
1	U.S. Geological Survey, Naval Weapons Plant
1	U.S. Geological Survey (Nolan)
1	U.S. Geological Survey, Washington
1	U.S. Geological Survey, WR Division
1	U.S. Mission to the International Atomic Energy Agency
1	U.S. Weather Bureau, Las Vegas
1	U.S. Weather Bureau, Washington
1	University of California (Libby)
2	University of California, Berkeley (Library)
4	University of California, Livermore (Library)
1	University of California, Livermore (Vay Shelton)
1	University of California, Los Angeles
1	University of California, Los Angeles (Larson)
1	University of Hawaii (Cox)
1	University of Rochester (Hempelmann)
1	University of Tennessee (UTA)
1	University of Washington (Donaldson)
1	University of Washington (Flemming)
1	Woods Hole Oceanographic Institute
1	Yale University (Sears)
25	Technical Information Extension, Oak Ridge

USNRDL

35	USNRDL, Technical Information Division

DISTRIBUTION DATE: 15 March 1963

Naval Radiological Defense Laboratory
USNRDL-TR-612 (DASA 1344)
HYDRA PROGRAM DETERMINATION OF THE TOTAL THERMAL RADIANT ENERGY EMITTED BY AN UNDERWATER EXPLODING WIRE by J. S. Hege
10 January 1963 33 p. tables illus. 5 refs.
UNCLASSIFIED

The total thermal radiation from an underwater spark has been determined by the measurement of the absolute radiation at two wavelengths as a function of time. Planck's law for thermal radiation was applied.

The spark was generated by electrically exploding a 5-mil. copper wire stretched between two submerged (over)

1. Underwater explosions.
2. Thermal radiation.
3. Emissivity.
4. Exploding wire phenomena.

I. Hege, J. S.
II. Title.

UNCLASSIFIED

Naval Radiological Defense Laboratory
USNRDL-TR-612 (DASA 1344)
HYDRA PROGRAM DETERMINATION OF THE TOTAL THERMAL RADIANT ENERGY EMITTED BY AN UNDERWATER EXPLODING WIRE by J. S. Hege
10 January 1963 33 p. tables illus. 5 refs.
UNCLASSIFIED

The total thermal radiation from an underwater spark has been determined by the measurement of the absolute radiation at two wavelengths as a function of time. Planck's law for thermal radiation was applied.

The spark was generated by electrically exploding a 5-mil. copper wire stretched between two submerged (over)

1. Underwater explosions.
2. Thermal radiation.
3. Emissivity.
4. Exploding wire phenomena.

I. Hege, J. S.
II. Title.

UNCLASSIFIED

electrodes. The spark was assumed to be cylindrical with its length determined by the length of the wire.

The light measurements were made with two calibrated photoelectric tubes. Wavelengths of 407 and 610 millimicrons were selected with Farrand interference filters.

Values for the rates of total thermal radiation and values for the spark temperatures and radii were tabulated and graphed as functions of time for three explosions under three different sets of conditions. Total thermal radiation was obtained by graphically integrating the rate of thermal radiation over the time of the process. For two of the three explosions approximately 30 percent of the spark energy was emitted as thermal radiation. It was not possible to determine this fraction for the third explosion.

Analysis of the propagation of error shows that the error in the results for total thermal radiation is less than 7.5 times any error in the measurements of the radiation incident on the photoelectric tubes. UNCLASSIFIED

electrodes. The spark was assumed to be cylindrical with its length determined by the length of the wire.

The light measurements were made with two calibrated photoelectric tubes. Wavelengths of 407 and 610 millimicrons were selected with Farrand interference filters.

Values for the rates of total thermal radiation and values for the spark temperatures and radii were tabulated and graphed as functions of time for three explosions under three different sets of conditions. Total thermal radiation was obtained by graphically integrating the rate of thermal radiation over the time of the process. For two of the three explosions approximately 30 percent of the spark energy was emitted as thermal radiation. It was not possible to determine this fraction for the third explosion.

Analysis of the propagation of error shows that the error in the results for total thermal radiation is less than 7.5 times any error in the measurements of the radiation incident on the photoelectric tubes. UNCLASSIFIED